Single-cell mechanics provides a sensitive and quantitative means for probing amyloid-β peptide and neuronal cell interactions

Valentin Lulevich[a], Christopher C. Zimmer[a], Hyun-seok Hong[b], Lee-way Jin[b,c,1], and Gang-yu Liu[a,1]

[a]Department of Chemistry, University of California, Davis, CA 95616; and [b]Medical Investigation of Neurodevelopmental Disorders Institute and [c]Department of Pathology and Laboratory Medicine, Alzheimer's Disease Center, University of California Davis Medical Center, Sacramento, CA 95817

Communicated by George W. Flynn, Department of Chemistry, Columbia University, New York, NY, June 23, 2010 (received for review December 8, 2009)

By using a highly sensitive technique of atomic force microscopy-based single-cell compression, the rigidity of cultured N2a and HT22 neuronal cells was measured as a function of amyloid-β42 (Aβ42) protein treatment. Aβ42 oligomers led to significant cellular stiffening; for example, 90–360% higher force was required to reach 80% deformation for N2a cells. Disaggregated or fibrillar forms of Aβ42 showed much less change. These observations were explained by a combination of two factors: (*i*) incorporation of oligomer into cellular membrane, which resulted in an increase in the Young's modulus of the membrane from 0.9 ± 0.4 to 1.85 ± 0.75 MPa for N2a cells and from 1.73 ± 0.90 to 5.5 ± 1.4 MPa for HT22 cells, and (*ii*) an increase in intracellular osmotic pressure (e.g., from 7 to 40 Pa for N2a cells) through unregulated ion influx. These findings and measurements provide a deeper, more characteristic, and quantitative insight into interactions between cells and Aβ42 oligomers, which have been considered the prime suspect for initiating neuronal dysfunction in Alzheimer's disease.

atomic force microscopy | Alzheimer's disease | cell mechanics | neuronal dysfunction | Young's moduli

Amyloid-β peptide (Aβ) is the major constituent of the fibrils deposited in amyloid plaques and cerebral blood vessels in patients with Alzheimer's disease (AD). Aβ accumulation in the brain and its neurotoxicity have been postulated to be the primary influence driving AD pathogenesis (1, 2). The Aβ peptide is produced by proteolytic cleavage of the transmembrane amyloid-β precursor protein (APP). Primary forms of Aβ, such as those of Aβ40 and Aβ42, self-aggregate to insoluble fibrils via a multistep process involving transient or metastable soluble intermediates, known as oligomers, protofibrils, amyloid pores, and AD diffusible ligands (1–3). Some of these aggregates may not be obligate intermediates in the fibril formation and can be stable (4, 5). Importantly, recent in vitro and in vivo studies have revealed that the build-up of soluble Aβ oligomers, rather than Aβ fibrils, may be an early and central event in the pathogenesis of AD (3, 6–9). The strong and rapidly disruptive effect of Aβ oligomers on synaptic and neuronal integrity is hypothesized to be a proximate cause of cognitive deficits in AD. The strongest support for this hypothesis comes from demonstrations that a form of soluble oligomers isolated from APP transgenic mice, called "Aβ*56," and low-*n* oligomers isolated from AD brains rapidly caused memory deficits when injected into naïve rats (6, 7).

The exact mechanism of Aβ oligomers' toxicity to neurons remains unknown. Aβ can have a major impact on neurons by interacting with the cell surface from extracellular space or by accumulating in intracellular organelles, such as multivesicular bodies or mitochondria (10–12). Irrespective of the cellular sites of attack, the neuronal damages appear to be initiated by the strong interactions between Aβ oligomers and membranes (13, 14). Aβ peptides are amphipathic and bind preferentially to membranes. Numerous studies have demonstrated detrimental effects of Aβ peptides on plasma membranes (13). The actions could include structural changes in cellular membrane caused by Aβ oligomers' absorption into membrane (15), ion pore creation (16, 17), binding with lipid rafts (18), enhanced membrane permeability or ion conductance (9), direct interaction with a wide array of ion channels (19), and osmotic pressure buildup in conjunction with unregulated ion flux (17, 19, 20). In principle, these proposed protein–membrane interactions would impact cellular mechanics in characteristic ways: membrane elastic compliance changes, increases in permeability, elasticity, heterogeneity, and a rise in osmotic pressure, respectively. Therefore, this work investigates if and how single-cell mechanics could provide a useful means to understand and quantify these interactions, using the most potent form, Aβ42.

The cellular mechanics were measured using our method of single-cell compression (21), from which force versus deformation profiles were acquired as a function of Aβ42 treatment. A schematic shown in Fig. 1 illustrates the concept. A cell is deformed between a flat glass substrate and a glass microsphere attached to the tip of an atomic force microscopy (AFM) probe. This technique was chosen over other methods mainly because of its quantitative nature, its high sensitivity to local pressures (0.1–1 Pa), and its ability to probe membrane, cytoskeleton, and other intracellular structures at the single-cell level. The results indicate that the measurement is sensitive to Aβ42 treatment and that it provides quantitative insights into the mechanism of the Aβ42–neuronal cell interaction.

Results

Single-Cell Mechanics of N2a Cells. Typical N2a cells (>85% of the population) exhibited a characteristic ellipsoidal shape with short neuritis (Fig. 2). They adhered to coverslips as individual entities instead of large colonies. The long and short axes ranged from 17 to 32 and 15 to 20 μm, respectively. The cell height is defined by the distance between the highest point above the nucleus and the glass substrate and is measured using AFM. The typical height ranged from 9 to 14 μm, corresponding well to known dimensions of neuronal cells (22).

Fig. 2*A* shows compression profiles for a typical N2a cell following three consecutive cycles. The N2a cell has a smooth and nonlinear deformation profile without irregularities or stress peaks, indicating its soft and pliable nature. A typical cell requires a force of 6.6 ± 2.8 nN to reach 30% deformation and a force of 235 ± 45 nN to reach 80% deformation (Table 1, row 1). Even at 90% deformation and 1-μN load, the cell remains viable, as demonstrated by trypan blue assay (23) shown in Fig. 2*B*.

The resilience of cells was tested via multiple compression cycles. After 2–3 min recovery time, the force profile in the second cycle remains almost identical to that in the first. Remarkably, the

Author contributions: L.-w.J. and G.-y.L. designed research; V.L., C.C.Z., and H.-s.H. performed research; V.L. and C.C.Z. analyzed data; and V.L., L.-w.J., and G.-y.L. wrote the paper.

The authors declare no conflict of interest.

[1]To whom correspondence should be addressed. E-mail: lee-way.jin@ucdmc.ucdavis.edu or liu@chem.ucdavis.edu.

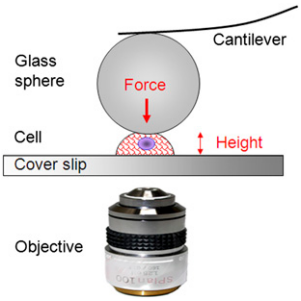

Fig. 1. Schematic diagram illustrating the methodology of single-cell compression.

cell recovered to its original height. The height for the cell shown in Fig. 2*A* initially measured 13.7 ± 0.2 μm and became 13.5 ± 0.2 μm after the first cycle. The cell remained viable and recovered to its original shape after the first and the second compression (Fig. 2*B*). The force profile for the third compression cycle remained very similar to the first (Fig. 2*A*) and showed only a 0.7-μm reduction in height. This behavior is characteristic and typical among N2a cells (≥95%).

Blebs were visible under optical microscopy and were more evident under fluorescence microscopy. When deformation exceeds 50% of the original height, cells typically develop one to nine blebs, ranging from 2–21 μm in diameter. Similar to previous reports, these blebs represent detachment of the plasma membrane from the cytoskeleton because of an increase in intracellular pressure under compression (24). As shown in the optical snapshots in Fig. 2*B*, blebs retracted within 1 or 2 min after unloading (note that to avoid the effect of dye on cell mechanics, all force values represented in this work were measured on cells without cell-tracing dye).

Single-Cell Mechanics of HT22 Neuronal Cells. To test if the above observation is cell type-specific, we further investigated HT22 cells, a murine central nervous system (CNS) neuronal line (25, 26). In contrast to the non-CNS neuroblastoma N2a cells, HT22 cells are derived from mouse hippocampus and therefore better represent brain neurons. Because HT22 cells, on average, are taller than N2a cells, only a subset of the population similar in size to N2a cells (14–17 μm in height and 15–25 μm in lateral dimensions) were chosen to assure a fair comparison.

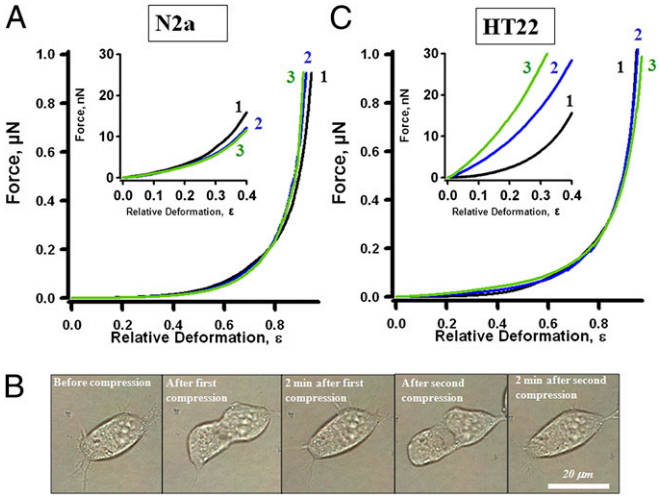

Fig. 2. (*A*) Three sequential force–deformation profiles of a typical N2a neuronal cell. Each compression cycle is numbered. *Inset* shows zoom-in at small deformations. (*B*) Optical snapshots of the N2a cell in *A* revealing the change in shape as a result of compression with a load up to 1 μN. (*C*) Three sequential force–deformation profiles for a typical HT22 neuronal cell.

Fig. 2*C* displays the deformation profiles for HT22 cells. As in N2a cells, the force profile during loading was smooth without stress peaks. HT22 cells also revealed one to seven blebs ranging in diameter from 4–15 μm at high deformation. These blebs retracted shortly after the load was removed. In contrast to N2a cells, sequential loading profiles revealed that HT22 cells stiffen slightly and became taller, especially at small deformation (Fig. 2*C*, *Inset*). For the cell shown in Fig. 2*C*, the height initially measured 14.2 ± 0.2 μm and became 15.3 ± 0.2 μm after the first load and 17.1 ± 0.2 μm after the second. Optical monitoring showed that shortly after compression HT22 cells minimized spreading and eventually balled up and detached. Quantitative information on HT22 cells is summarized in Table 1, row 6.

This behavior of N2a and HT22 cells is in sharp contrast to many other cells, such as (*i*) T lymphocytes, which burst beyond 30% deformation (21), and (*ii*) the human breast cancer cell line MDA-MB-468 and the normal prostatic epithelial cell line MLC-SV40, which do not recover if the deformation exceeds 50–60% (24). Even without bursting, robust cells such as keratinocytes do not remain viable after the first compression, despite the recovery of cell height (21). Therefore, we conclude that high pliability and resilience are characteristics of these neuronal cells.

Aβ Oligomer–Cell Interactions as Probed by Single-Cell Mechanics. A comparison of typical force–deformation profiles for N2a cells, with and without treatment of Aβ42 oligomer, is shown in Fig. 3*A*. Cells appear more rigid than the control after 30 min of treatment. A load of 21 ± 14 nN is needed to deform N2a cells to 30% deformation, and 535 ± 315 nN is required to reach 80%. This increase is, on average, 230% at 30% deformation and 130% at 80% deformation. To ensure the potency of oligomers, parallel cultures were used for a (3-(4,5-dimethylthiazol-2-yl)-2,5-diphenyltetrazolium bromide) formazan exocytosis (MTT-FE) assay. We previously designed this assay for rapid evaluation of the cellular toxicity of Aβ oligomers (27). A positive MTT-FE response is a reliable indication of cellular toxicity induced by low (micromolar) concentrations of Aβ oligomer (27). MTT-FE assays revealed Aβ oligomer-induced neurotoxicity in more than 90% of cells. Consistently, more than 90% of Aβ42 oligomer-treated cells exhibit increased rigidity. Similar to controls, oligomer-treated cells developed blebs during compression. In contrast to controls, it took longer for these blebs to retract after removal of load, so that many blebs remained visible even 2 min after unloading. To enhance the visibility and to quantify the blebs, parallel compression experiments were carried out for cells treated for 30 min with 5 μM of CellTracker green. When deformation exceeds 50% of the original height, oligomer-treated N2a cells typically develop two to eight blebs, ranging in diameter from 3 to 17 μm.

Increased rigidity also was observed in oligomer-treated HT22 cells, as shown in Fig. 3*B*. A load of 32 ± 20 nN is needed to deform oligomer-treated HT22 cells to 30% deformation, and a load of 602 ± 172 nN is required to reach 80%, indicating increases of 280% and 150% at 30% and 80% deformation, respectively. Quantifications for HT22 cells are shown in Table 1, row 7. At high deformation, oligomer-treated HT22 cells typically develop one to three blebs, ranging from 5 to 16 μm in diameter.

The Aβ oligomer stiffening of neuronal cells is dynamic, as evidenced by the requirement of the presence of oligomers in solution. In the experiments shown in Fig. 3*C*, N2a cells were treated for 30 min with oligomer. Immediately before the compression experiment, the cells were washed to remove oligomers and were cultured in fresh medium. Results shown in Fig. 3*C* indicate little stiffening had taken place; instead, cells appeared to have undergone almost complete recovery (Table 1, row 3). This observation suggests that alterations of cell mechanics require the continuous presence of Aβ oligomer and are reversible after disengagement of Aβ oligomer. This behavior is analogous to a chemical reaction equilibrium, which appears steady as dictated by its equilibrium constant but is dynamic at the mo-

Table 1. Comparison of mechanical properties of neuronal cells before and after treatment by various forms of Aβ peptide

Index	Cell and treatment	Force (nN) at ε = 0.3	Force (nN) at ε = 0.8	Aβ oligomer cytotoxicity via MTT-FE assay	E_m (MPa)	ΔC (μM)
1	N2a, control	6.6 ± 2.8	235 ± 45	N/A	0.9 ± 0.4	N/A
2	N2a, treated by Aβ oligomer	20.5 ± 14.5	535 ± 315	>90%	1.85 ± 0.75	20 ± 15
3	N2a, treated by Aβ oligomer and replaced with medium before compression	8.3 ± 7.9	234 ± 67	>90%	1.1 ± 0.5	1.9 ± 13
4	N2a, treated by Aβ monomer	6.5 ± 2.5	275 ± 70	<10%	1.1 ± 0.4	0.1 ± 5
5	N2a, treated by fibrillar Aβ	14 ± 5	280 ± 70	<30%	1.5 ± 0.4	11 ± 8.9
6	HT22, control	8.5 ± 3.5	245 ± 65	N/A	1.73 ± 0.90	N/A
7	HT22, treated by Aβ oligomer	32 ± 20	602 ± 172	>90%	5.5 ± 1.4	34 ± 24
8	Jurkat Tl lymphoma cells (21)	23 ± 3	200 ± 100	N/A	23 ± 13	N/A

lecular level and thus will shift when reaction conditions, such as concentration or temperature (chapter 9 of ref. 28), are changed. The corresponding MTT-FE assay showed that the 30-min treatment followed by protein removal resulted in the same MTT-FE response seen in cultures with continuous presence of Aβ42 oligomer. Therefore, despite the transient and dynamic nature of membrane structural change induced by short-term Aβ oligomer treatment, it appears that 30 min of interaction with the membrane causes sustained internal damage that is not reversible, even though the membrane mechanics appear normal upon removal of oligomers.

The amyloid dye Congo red (CR) is known to recognize the amyloid conformation of Aβ oligomers and inhibit their toxicity (27, 29–32). We added CR into our protocol to investigate whether it would block or reverse the oligomer effect on cell mechanics (27, 32). CR (25 μM) itself did not alter the mechanics of N2a cells. Premixing 5 μM Aβ oligomer with 25 μM CR resulted in substantially reduced cell stiffening. Force–deformation profiles for cells treated with the oligomer-CR mixture are shown along with untreated cells in Fig. 3*D*. The load measured 10 ± 6 nN at 30% deformation and 286 ± 62 nN at 80% deformation, reflecting a 60% reduction in Aβ oligomer impact on single-cell mechanics. Doubling the CR concentration (i.e., 50 μM; CR:Aβ42 = 10:1) almost completely diminished the cellular stiffening. The results are reproducible, as tested in 70 cells and in three independent experiments. Parallel rapid MTT-FE assays showed that CR was able to reduce the oligomer toxicity, as evidenced by the reduction of the affected cells from 90% to 10–30% at a CR:oligomer ratio of 5:1 and to 10%, at a CR:oligomer ratio of 10:1. Therefore, we conclude that the amyloid conformation of Aβ oligomer is required for the increase in the cell's elastic compliance and that the stiffening correlates well with the cytotoxicity.

In addition, the dynamic nature of this interaction provides a hint for new therapeutic tactics, at least during the initial oligomer–neuronal cell interactions. A very simple concept is the attempt to reverse the effect by adding CR immediately after 30-min incubation with 5-μM oligomer, which remains in the cell-culture medium. At a sufficient CR concentration (e.g., 25 μM), the load measured 7 ± 5 nN at 30% deformation and 287 ± 82 nN at 80% deformation. This result indicated an average 81% reduction in the oligomers' impact. The reduced effect seen with the subsequent addition of CR may reflect, in part, the strong binding affinity of CR for Aβ42 (27, 29–32). It is possible that CR targets oligomers exposed within the openings of newly created ion pores (16, 17), thus blocking and slowing the influx of ions.

Disaggregated Aβ and Aβ Fibrils Reveal Much Less Impact on N2a Cell Mechanics. To understand the mechanism of Aβ oligomer–neuronal

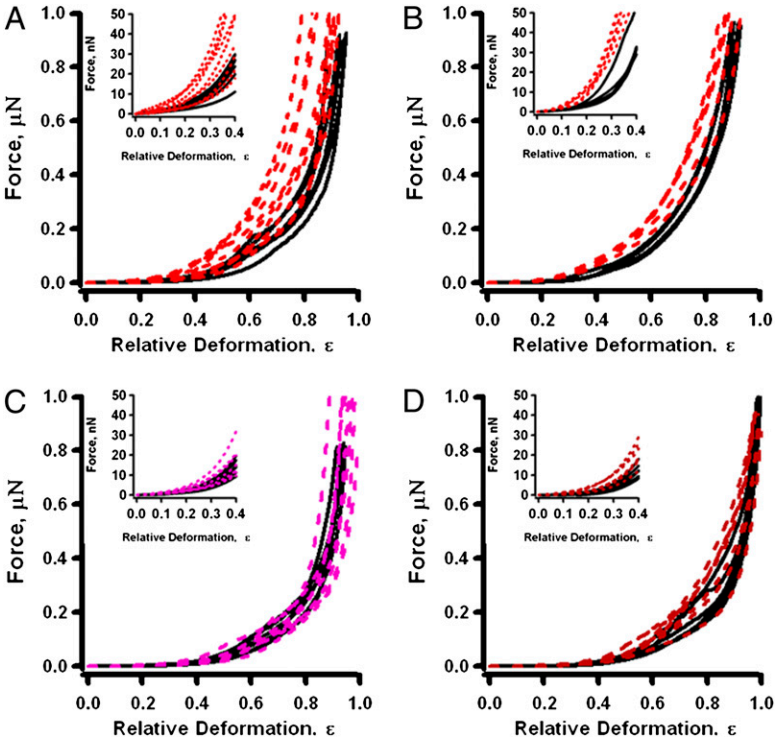

Fig. 3. (*A*) Typical force–deformation profiles for control N2a neuronal cells (solid black lines) and for N2a neuronal cells treated by Aβ oligomer (dashed red lines). Each curve was taken from a live cell. (*B*) Typical force–deformation profiles for oligomer-treated (dashed red lines) and control (solid black lines) HT22 cells. (*C*) Measurements similar to those in *A*, except that Aβ oligomers were removed after 30 min. Dashed purple lines indicate oligomer-treated N2a cells, (*D*) Measurements similar to those in *A*, except that the 5-μM Aβ oligomer was mixed with 25-μM Congo red (dashed red line) before N2a cell treatment. *Insets* reveal more clearly the cellular mechanics at small deformations.

cell interaction, we first considered the possibility that Aβ42 molecules physisorbed onto the plasma membrane; this process would reduce fluidity and increase membrane thickness and, therefore, stiffness. Thus, disaggregated and fibrillar forms would exhibit similar effects. The stiffening potency should follow disaggregated > oligomer > fibrillar, taking solubility into consideration, also.

Typical force profiles for N2a cells after 30-min treatment with disaggregated Aβ are shown in Fig. 4*A*. The overall profiles for these cells reveal strong similarities with the control: A force of 6.5 ± 2.5 nN is required for 30% deformation, and a force of 275 ± 70 nN is required to reach 80% deformation (Table 1, row 4). The stiffening effect is only 4–17%. This result correlates well with simultaneous MTT-FE assays, which showed less than 10% cytotoxicity.

Although force profiles under fibrillar Aβ treatment are difficult to measure because of the higher level of noise caused by large aggregates in solution, the profiles were acquired, and typical force profiles are shown in Fig. 3*B*. The overall trends were similar to those in the control, and fibrils did cause small stiffening, especially at small deformations. A force of 14 ± 5 nN was required to deform N2a at 30%, and 280 ± 70 nN was required to compress height by 80% (Table 1, row 5). Greater stiffening at small deformations may be attributed to the difficulties in finding the contact point, as caused by large aggregates. Despite this difficulty, cells treated with the fibrillar form were only 20% stiffer than the control. This result also correlates well with simultaneous MTT-FE assays, which showed only 30% cytotoxicity (27).

Taken collectively, these results indicate that physisorption alone does not adequately explain the observation that the oligomeric form of Aβ42 exhibited the largest stiffening in cell mechanics and the highest toxicity. The protein molecules therefore are likely to intercalate into the cellular membrane. This conclusion is consistent with prior knowledge that the Aβ42 oligomer binds with high affinity with various membrane components, such as the outer envelope of polar headgroups, ganglioside clusters in raftlike structures, insulin receptors, $\alpha_5\beta_1$ integrin, and α7nAChR protein, to name a few (14, 18, 33).

Quantification of Apparent Young's Modulus of the Cellular Membrane. A simple analytical formula was derived from the elastic theory of membranes to quantify deformation profiles and to extract the membrane's Young's modulus, E_m (21). Under assumptions *i–iii* below, the force, F, is calculated by Eq. **1**:

$$F_m = 2\pi \frac{E_m}{1-\nu_m} h R_0 \varepsilon^3 \qquad [1]$$

where ε represents relative deformation, and ν_m is the Poisson ratio. Here, R_0 and h are the radius of the uncompressed cell and its plasma membrane thickness, respectively.

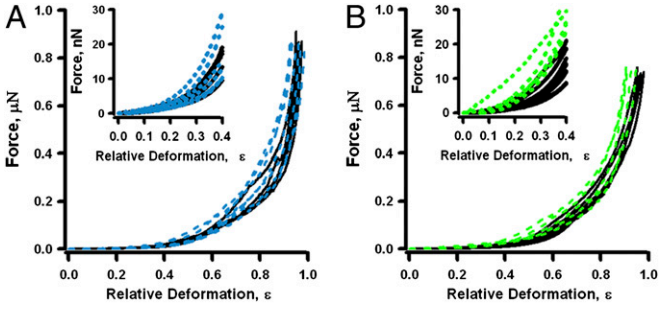

Fig. 4. (*A*) Typical force–relative deformation profiles for control N2a neuronal cells (solid black lines) and for N2a neuronal cells upon addition of Aβ monomer (dashed blue lines). (*B*) Typical force–relative deformation profiles for control N2a neuronal cell (solid black lines) and N2a neuronal cells treated with fibrillar Aβ peptide (dashed green lines). *Insets* are zoom-in at small deformations.

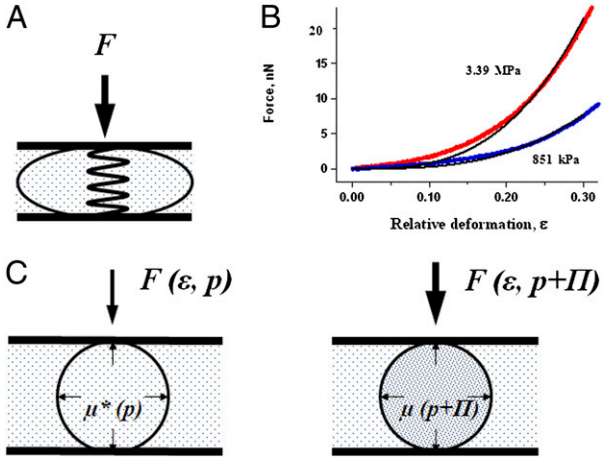

Fig. 5. (*A*) Schematic of the balloon model, in which external force causes the membrane to stretch and bend. (*B*) Nonlinear fitting to Eq. **1** from profiles of a control (blue) and an Aβ oligomer-treated (red) N2a cell. (*C*) Schematic diagram illustrating the impact of intracellular ions. Control is represented by a normal physiological pressure, p, and a cytoplasmic chemical potential, $\mu^*_A(p)$. Osmotic pressure, Π, would be present because of the increased intracellular ion concentration, leading to a chemical potential change; accordingly, $\mu_A(p + \Pi)$ (28).

This model is based on the following assumptions: (*i*) cells may be treated as a spherical membrane (balloon) filled with an incompressible fluid, sandwiched between two parallel plates, as shown in Fig. 5*A*; (*ii*) the membrane is impermeable; and (*iii*) the contribution from other cellular components is negligible at low deformation (ε <30%).

The first assumption arises from the fact that the probe is larger than the cell height. The second assumption is based on prior experiments (23) and single-cell mechanics of T cells (21). The third assumption arises from the known fact that neuronal cells have a relatively weak cytoskeleton (34, 35), and the nuclear contribution is not significant because of the lack of contrast in Young's modulus between the cytoskeleton and nucleus (36). More accurate models and advanced calculation methods such as finite element analysis may be necessary to account for profiles at higher deformation. For this work, this model works sufficiently well at low deformation and, therefore, enables quantification of E_m.

Least squares fitting to force–deformation profiles using Eq. **1** results in E_m = 0.9 ± 0.4 MPa for N2A cells. After oligomer treatments, E_m = 1.85 ± 0.75 MPa. Fig. 5*B* shows two typical fits at ε = 0–30% for a treated ($\chi^2 = 6 \times 10^{-16}$) and an untreated ($\chi^2 = 2 \times 10^{-16}$) N2a cell. The E_m for HT22 cells is 1.73 ± 0.90 MPa and increases to 5.5 ±1.4 MPa upon Aβ42 treatment. The good quality of fitting can be seen in Fig. 5, as well as by the low χ^2 values ($9 \times 10^{-17} - 4 \times 10^{-15}$)[†] The values reported in Table 1 represent the average E_m in the specified experiment, and the uncertainty indicates the variation or individuality of cells.

Estimation of Increase in Intracellular Ion Concentration as a Result of Aβ Oligomer Treatments. Assuming the change in concentration of intracellular ions is solely responsible for the stiffening, the force balance between load and osmotic pressure yields Eq. **2**:

$$\Delta F = \Pi \cdot S \qquad [2]$$

where ΔF, Π, and S are excess force, increase in osmotic pressure, and cell-probe contact area, respectively. The contact area,

[†]Note: The uncertainty of E_m for each fit arises from (*i*) errors in determining deformation and force, which are insignificant, and (*ii*) deviation from the analytical model, which depends on the behavior of cells.

S, at small deformation between the glass bead and hemispherical cell can be estimated using Eq. **3**:

$$S = 2\pi R^2 \varepsilon \quad [3]$$

where R is the contact radius. In this configuration, R is approximately equal to cell height, H. A typical N2a cell has a height of 12 μm, and $\varepsilon = 0.3$; thus, Eq. **3** results in $S = 2.7 \times 10^{-10}$ m^2. Taking an average $\Delta F = 15$ nN at $\varepsilon = 30\%$, the osmotic pressure increase, Π, necessary to account for cell stiffening, is estimated to be 50 Pa. For HT22 cells, $\Delta F = 24$ nN; $\Pi = 150 \pm 126$ Pa.

From the relationship between osmotic pressure and ion concentration (28), one can calculate the molar concentration increase in intracellular ions, ΔC, via Eq. **4**:

$$\Delta C = \frac{\Pi}{RT} \quad [4]$$

where R is the gas constant, and T is the temperature. At $\varepsilon = 30\%$, the Aβ42 treatment could lead to an intracellular ion concentration increase of 20 ± 15 μM in N2a cells, and 34 ± 24 μM in HT22 cells. Fig. 5*C* illustrates the change in osmotic pressure caused by an unregulated increase in intracellular ion concentration in terms of the chemical potential of the cytoplasm of the cell. The estimated ΔC for treatment with each form of Aβ42 is reported in Table 1.

Discussion

Our results suggest that soluble Aβ42 exhibits a strong impact on N2a cell mechanics, e.g., a 130%, 17%, and 20% increase in force at 80% deformation for oligomeric, disaggregated, and fibrillar forms, respectively. This result correlates well with the cytotoxicity measured in MTT-FE assays, where 90%, 10%, and 25% fatalities were reported, respectively. The same trend also was observed for HT22 cells. The trend may be explained by increase in osmotic pressure. However, this process must compete with the loss of ions and cellular fluid through a membrane which has been compromised by the oligomer, whether by nonendogenous channels or larger discontinuities such as those previously reported in the literature (9, 16, 17, 37, 38). Therefore, we conclude that any effect caused by increased membrane permeability that might be responsible for the loss of cellular content must be small in comparison with the effect of the change in osmotic pressure, so that the change in osmotic pressure dominates the change in cell mechanics.

To quantify contributions further, we separate (*i*) the binding of Aβ oligomers to various membrane components (such as the outer envelope of polar headgroups, ganglioside clusters in rafts, insulin receptors, $\alpha_5\beta_1$ integrin, and α7nAChR protein, to name a few) (14, 18, 33), and (*ii*) the treatment that alters membrane permeability by changing ion channels or making new pores, resulting in increased intracellular ion concentration. The former reduces fluidity and increases spring constant; the latter leads to greater osmotic pressure, which manifests into stiffer force–deformation profiles.

In case *i*, the observation is solely the result of membrane stiffening. Least squares fitting using Eq. **1**, reveals an increase in E_m by 105%, on average, for N2a cells and 220% for HT22 cells; both values are considered significant in membrane mechanics. Direct comparison of the impact on cell mechanics and MTT-FE assay indicates that the oligomeric form exhibits the highest increase in single-cell mechanics and the highest potency in neuronal toxicity. As discussed in the previous section, this finding suggests that the interaction between Aβ and cells is intrinsically greater than can be explained simply by physisorption onto membrane surfaces. During the process of self-aggregation, Aβ peptides generate hydrogen peroxide and hydroxyl radicals, which may induce the formation of covalent bonds between membrane proteins and lipids (2). If that process occurs in Aβ42-treated cells, membrane stiffening should be permanent. Our experiments, however, indicate that the oligomer-induced stiffness is reversible, at least at the beginning of treatment. Therefore, this investigation supports the previous hypothesis that Aβ42 oligomers insert into cellular membrane because of their affinity for various membrane components, such as proteins and rafts. These merging processes could be dynamic, as demonstrated by the pseudoequilibrium behavior at the beginning of the interactions.

In case *ii*, an increase in intracellular osmotic pressure is solely responsible for the observation. ΔC is calculated to be 20 ± 15 μM for N2a cells and 34 ± 24 μM for HT22 cells. Note that the observed stiffening is not caused solely by ΔP; therefore the ΔC value represents the upper limit. Because neither Aβ monomers nor fibrils contribute to the increase in Ca^{2+} level (17), the observed increase could be caused by the presence of minute amounts of oligomer from the disaggregation of fibers. Prior studies reported that treatment with Aβ oligomer increases the intracellular Ca^{2+} level by only 0.2–1 μM, depending on treatment and cells used (17, 20), a value that is ≈20 times less than our ΔC. This comparison suggests that the increased rigidity cannot be associated solely with Ca^{2+} flux and very likely involves other ions (38, 39).

Taken collectively, these considerations suggest that the observed increase in rigidity probably is caused by a combination of (*i*) oligomer insertion into various membrane components, and (*ii*) an increase in intracellular ion concentration or osmotic pressure. Incorporation of Aβ oligomers into membrane not only reduces fluidity or increases elasticity but also increases permeability, causing deregulation of or an increase in the intracellular ion concentration and eventual cell death.

Single-cell mechanics in terms of force–deformation profiles provides a sensitive and quantitative way to characterize Aβ42–neuronal cell interactions. Recently, experimental therapies targeting membranes have gained promise (13). Examples include docosahexaenoic acid, a polyunsaturated fatty acid that has been known to have a profound effect on membrane properties and to protect neurons from amyloid toxicity (39). A very recent article reports the use of poloxamer 188 as a membrane sealant to repair the Aβ oligomer-damaged membranes (40). Our method would be useful for screening therapeutic molecules and characterizing their effects on remedying Aβ–membrane interactions.

Materials and Methods

Cell Preparation. N2a neuroblastoma cells were cultured in a mixture of 50% (vol/vol) DMEM (Invitrogen) and 50% GIBCO Opti-MEM I reduced serum medium (Invitrogen) supplemented with 5% FBS (Invitrogen) and 0.5% penicillin/streptomycin (Invitrogen). For cell plating, the cultures were washed once with PBS (pH, 7.4) and harvested by trypsinization. Cells were spun down at $859 \times g$ for 3 min. The cell pellet was resuspended to 1×10^4 cells/mL; then 2 mL of the suspension was deposited in a glass-bottomed Petri dish (MatTek). Plated samples were cultured (37 °C, 5% CO_2) for 48 h to facilitate attachment. Before cell compression, the medium was removed, and the cells were rinsed three times with PBS buffer and then were suspended in serum-free Opti-MEM. HT22 hippocampal neuronal cells were cultured using the same procedure. Treatment by design forms of Aβ was done by incubation in 5 μM peptide (50% PBS/Opti-MEM) for 30 min. For trypan blue (Invitrogen) assay or cellTracker green (Invitrogen) tagging, cells were incubated in 5 μM dye medium for 30 min, followed by 45 min in medium, rinsed with PBS buffer, and stored in medium.

Preparation of Disaggregated, Oligomeric, and Fibrillar Aβ42 Solutions. Aβ peptides were purchased from American Peptide. Solutions of disaggregated Aβ and Aβ42 oligomers were made of synthetic Aβ1–42 peptide, using a previously established protocol (7, 14, 22), to form "prefibrillar oligomers" (5). These Aβ oligomers have been characterized extensively in our previous studies (14, 22). The assemblies range from tetrameric up to ~75 kDa in size (5). To ensure consistent quality, a random sample from each batch was imaged using transmission electron microscopy (27). The average diameter of the spherical oligomers measured 6.4 nm, and that of the fibrils was 10.3 nm.

Rapid MTT-FE Assay. Using our previous procedure (27), the rapid MTT-FE assay was used to determine quickly the level of cytotoxicity induced by Aβ42. Cells were plated at a density of 20,000 cells/well in 96-well plates. Each well had 100 μL of Opti-MEM, and the plates were incubated at 37 °C

with 5% CO_2 for 12–24 h; then defined Aβ42 was added. After incubation for 1 h with the Aβ42, 0.5 mg/mL MTT (Sigma-Aldrich) was added and incubated for 1 h. At the end of incubation, the cells exocytosing MTT formazan were counted (41).

Congo Red Interference with Aβ42 Toxicity. CR was purchased from Sigma-Aldrich Corp. CR and Aβ42 oligomer solutions were premixed at a concentration ratio of 5:1 or 10:1 for 5 min to allow CR to bind to the oligomer. The final concentration for CR was kept at 25 μM.

Single-Cell Compression. The details for single-cell compression were reported previously (21) and are shown schematically in Fig. 1. Single-cell compression was measured with an MFP-3D AFM (Asylum Research Corp.). We attained 1-nN sensitivity over a broad force range (1 nN to 5 μN), using a 2-N/m cantilever (AC240; Olympus). An inverted IX50 optical microscope (Olympus America) was used in conjunction with the AFM to guide alignment. Glass spheres (40-μm diameter; Duke Scientific) were glued to the apex of AFM tips. The final k was determined via the added -mass method (42). Force–deformation curves were acquired on the bare surface near to obtain a reference point for measuring the cell's height and to determine substrate contribution.[‡]

Force–deformation profiles were plotted as loading force versus relative cell deformation, ε = cell height change/initial height. The probe–cell contact was determined by the kink point between the initial approach (linear) and the cell deformation portion (3/2 power law). To avoid hydrodynamic contribution, the approach speed was kept low, 2 μm/s (43). The load is calculated via $F = k \cdot \Delta$, where k is the probe's force constant, and Δ represents the cantilever deflection.

For each designed set of conditions, two or three sets of measurements were taken. In each set, 4–10 healthy cells were chosen. This work reports results of more than75 control and 93 Aβ–treated N2a cells, as well as 18 control and 27 treated HT22 cells. The force values in Table 1 are average ± SD. For N2a cells, the t test, performed at ε = 30% and 80%, resulted in t = 6.3 at both points, showing there is no similarity among the treated and untreated cells; the statistical difference is 99.9% (α = 0.001) (44, 45). For HT22 cells at ε = 30% and 80%, t = 4.6 and 7.7, respectively, again confirming that the stiffening effect is statistically true (>99.9%).

ACKNOWLEDGMENTS. We thank I. Maezawa, A. Hicklin, and S. Hilt for their technical assistance, R. H. Cheng for help in transmission electron microscopy, and C. Koehler and S. Stagner for proofreading. This work was supported by the University of California at Davis, by Pilot Grant AG010129 from the University of California at Davis Alzheimer's Disease Center, and by Grants 1R21 GM077850-01, 1R01 AG025500, and 1R21 AG031362 from the National Institute of Health.

[‡]Note: Using large glass spheres, glass substrates, and loads below 5 μN, the deformation from substrate is insignificant, a result that is consistent with the knowledge of elasticity: Glass = 50–90 GPa, and cells = 10 KPa–5 MPa.

1. Hardy J, Selkoe DJ (2002) The amyloid hypothesis of Alzheimer's disease: Progress and problems on the road to therapeutics. *Science* 297:353–356.
2. Mattson MP (2004) Pathways towards and away from Alzheimer's disease. *Nature* 430:631–639.
3. Caughey B, Lansbury PT (2003) Protofibrils, pores, fibrils, and neurodegeneration: Separating the responsible protein aggregates from the innocent bystanders. *Annu Rev Neurosci* 26:267–298.
4. Necula M, Kayed R, Milton S, Glabe CG (2007) Small molecule inhibitors of aggregation indicate that amyloid beta oligomerization and fibrillization pathways are independent and distinct. *J Biol Chem* 282:10311–10324.
5. Glabe CG (2008) Structural classification of toxic amyloid oligomers. *J Biol Chem* 283: 29639–29643.
6. Lesné S, et al. (2006) A specific amyloid-beta protein assembly in the brain impairs memory. *Nature* 440:352–357.
7. Shankar GM, et al. (2008) Amyloid-beta protein dimers isolated directly from Alzheimer's brains impair synaptic plasticity and memory. *Nat Med* 14:837–842.
8. Klein WL, Stine WB, Jr, Teplow DB (2004) Small assemblies of unmodified amyloid beta-protein are the proximate neurotoxin in Alzheimer's disease. *Neurobiol Aging* 25:569–580.
9. Kayed R, et al. (2004) Permeabilization of lipid bilayers is a common conformation-dependent activity of soluble amyloid oligomers in protein misfolding diseases. *J Biol Chem* 279:46363–46366.
10. LaFerla FM, Green KN, Oddo S (2007) Intracellular amyloid-beta in Alzheimer's disease. *Nat Rev Neurosci* 8:499–509.
11. Almeida CG, Takahashi RH, Gouras GK (2006) Beta-amyloid accumulation impairs multivesicular body sorting by inhibiting the ubiquitin-proteasome system. *J Neurosci* 26:4277–4288.
12. Caspersen C, et al. (2005) Mitochondrial Abeta: A potential focal point for neuronal metabolic dysfunction in Alzheimer's disease. *FASEB J* 19:2040–2041.
13. Talaga P, Quéré L (2002) The plasma membrane: A target and hurdle for the development of anti-Abeta drugs? *Curr Drug Targets CNS Neurol Disord* 1:567–574.
14. Verdier Y, Zarándi M, Penke B (2004) Amyloid beta-peptide interactions with neuronal and glial cell plasma membrane: Binding sites and implications for Alzheimer's disease. *J Pept Sci* 10:229–248.
15. Kremer JJ, Pallitto MM, Sklansky DJ, Murphy RM (2000) Correlation of beta-amyloid aggregate size and hydrophobicity with decreased bilayer fluidity of model membranes. *Biochemistry* 39:10309–10318.
16. Quist A, et al. (2005) Amyloid ion channels: A common structural link for protein-misfolding disease. *Proc Natl Acad Sci USA* 102:10427–10432.
17. Demuro A, et al. (2005) Calcium dysregulation and membrane disruption as a ubiquitous neurotoxic mechanism of soluble amyloid oligomers. *J Biol Chem* 280: 17294–17300.
18. Kakio A, Nishimoto S, Yanagisawa K, Kozutsumi Y, Matsuzaki K (2002) Interactions of amyloid beta-protein with various gangliosides in raft-like membranes: Importance of GM1 ganglioside-bound form as an endogenous seed for Alzheimer amyloid. *Biochemistry* 41:7385–7390.
19. Demuro A, Parker I, Stutzmann GE (2010) Calcium signaling and amyloid toxicity in Alzheimer disease. *J Biol Chem* 285:12463–12468.
20. Mattson MP, Chan SL (2003) Neuronal and glial calcium signaling in Alzheimer's disease. *Cell Calcium* 34:385–397.
21. Lulevich V, Zink T, Chen HY, Liu FT, Liu GY (2006) Cell mechanics using atomic force microscopy-based single-cell compression. *Langmuir* 22:8151–8155.
22. Groves PM, Rebec GV (1988) *Introduction to Biological Psychology* (W.C. Brown, Dubuque, IA), 3rd Ed.
23. Karp G (2003) *Cell and Molecular Biology* (Wiley., New York), p 740.
24. Lulevich V, Shih YP, Lo SH, Liu GY (2009) Cell tracing dyes significantly change single cell mechanics. *J Phys Chem B* 113:6511–6519.
25. Morimoto BH, Koshland DE, Jr (1990) Induction and expression of long- and short-term neurosecretory potentiation in a neural cell line. *Neuron* 5:875–880.
26. Davis JB, Maher P (1994) Protein kinase C activation inhibits glutamate-induced cytotoxicity in a neuronal cell line. *Brain Res* 652:169–173.
27. Hong HS, et al. (2007) Combining the rapid MTT formazan exocytosis assay and the MC65 protection assay led to the discovery of carbazole analogs as small molecule inhibitors of Abeta oligomer-induced cytotoxicity. *Brain Res* 1130:223–234.
28. Atkins PW (1998) *Physical Chemistry* (Oxford Univ. Press, Oxford), 6th Ed.
29. Lorenzo A, Yankner BA (1994) Beta-amyloid neurotoxicity requires fibril formation and is inhibited by congo red. *Proc Natl Acad Sci USA* 91:12243–12247.
30. Podlisny MB, et al. (1998) Oligomerization of endogenous and synthetic amyloid beta-protein at nanomolar levels in cell culture and stabilization of monomer by Congo red. *Biochemistry* 37:3602–3611.
31. Liu Y, Schubert D (2006) Treating Alzheimer's disease by inactivating bioactive amyloid beta peptide. *Curr Alzheimer Res* 3:129–135.
32. Maezawa I, et al. (2008) Congo red and thioflavin-T analogs detect Abeta oligomers. *J Neurochem* 104:457–468.
33. Terzi E, Hölzemann G, Seelig J (1997) Interaction of Alzheimer beta-amyloid peptide (1-40) with lipid membranes. *Biochemistry* 36:14845–14852.
34. Dai J, Sheetz MP, Wan X, Morris CE (1998) Membrane tension in swelling and shrinking molluscan neurons. *J Neurosci* 18:6681–6692.
35. Titushkin I, Cho M (2009) Regulation of cell cytoskeleton and membrane mechanics by electric field: Role of linker proteins. *Biophys J* 96:717–728.
36. Dahl KN, Engler AJ, Pajerowski JD, Discher DE (2005) Power-law rheology of isolated nuclei with deformation mapping of nuclear substructures. *Biophys J* 89:2855–2864.
37. Arispe N, Rojas E, Pollard HB (1993) Alzheimer disease amyloid beta protein forms calcium channels in bilayer membranes: Blockade by tromethamine and aluminum. *Proc Natl Acad Sci USA* 90:567–571.
38. Kourie JI, Henry CL, Farrelly P (2001) Diversity of amyloid beta protein fragment [1-40]-formed channels. *Cell Mol Neurobiol* 21:255–284.
39. Cole GM, Frautschy SA (2006) Docosahexaenoic acid protects from amyloid and dendritic pathology in an Alzheimer's disease mouse model. *Nutr Health* 18:249–259.
40. Mina EW, Lasagna-Reeves C, Glabe CG, Kayed R (2009) Poloxamer 188 copolymer membrane sealant rescues toxicity of amyloid oligomers in vitro. *J Mol Biol* 391: 577–585.
41. Liu Y, Schubert D (1997) Cytotoxic amyloid peptides inhibit cellular 3-(4,5-dimethylthiazol-2-yl)-2,5-diphenyltetrazolium bromide (MTT) reduction by enhancing MTT formazan exocytosis. *J Neurochem* 69:2285–2293.
42. Cleveland JPM, Bocek D, Hansma PK (1993) A nondestructive method for determining the spring constant of cantilevers. *Rev Sci Instrum* 64:403–405.
43. Lulevich VV, Vinogradova OI (2004) Effect of pH and salt on the stiffness of polyelectrolyte multilayer microcapsules. *Langmuir* 20:2874–2878.
44. Trochim WM. The Research Methods Knowledge Base. Available at: http://www.socialresearchmethods.net/kb/, Last Accessed: 7/5/2010.
45. Sternstein M (1996) *Statistics*, Barron's Educational Series; (Barron's; Hauppauge, NY).